Active Damping of Rotating Positioning Platforms using Force Feedback

T. Dehaeze [1,3], **C. Collette** [1,2]
[1] Precision Mechatronics Laboratory
University of Liege, Belgium

[2] BEAMS Department
Free University of Brussels, Belgium

[3] European Synchrotron Radiation Facility
Grenoble, France e-mail: **thomas.dehaeze@esrf.fr**

Abstract
Abstract text to be done

1 Introduction

Due to gyroscopic effects, the guaranteed robustness properties of Integral Force Feedback do not hold. Either the control architecture can be slightly modified or mechanical changes in the system can be performed. This paper has been published The Matlab code that was use to obtain the results are available in [1].

2 Dynamics of Rotating Positioning Platforms

2.1 Model of a Rotating Positioning Platform

In order to study how the rotation of a positioning platforms does affect the use of force feedback, a simple model of an X-Y positioning stage on top of a rotating stage is developed.

The model is schematically represented in Figure 1 and forms the simplest system where gyroscopic forces can be studied.

The rotating stage is supposed to be ideal, meaning it induces a perfect rotation $\theta(t) = \Omega t$ where Ω is the rotational speed in $\mathrm{rad\,s^{-1}}$.

The parallel X-Y positioning stage consists of two orthogonal actuators represented by three elements in parallel:

- a spring with a stiffness k in $\mathrm{N\,m^{-1}}$
- a dashpot with a damping coefficient c in $\mathrm{N\,m^{-1}\,s}$
- an ideal force source F_u, F_v

A payload with a mass m in kg is mounted on the rotating X-Y stage.

Two reference frames are used:

- an inertial frame $(\vec{i}_x, \vec{i}_y, \vec{i}_z)$

- a uniform rotating frame $(\vec{i}_u, \vec{i}_v, \vec{i}_w)$ rigidly fixed on top of the rotating stage. $\vec{i}_w$ is aligned with the rotation axis

The position of the payload is represented by (d_u, d_v) expressed in the rotating frame.

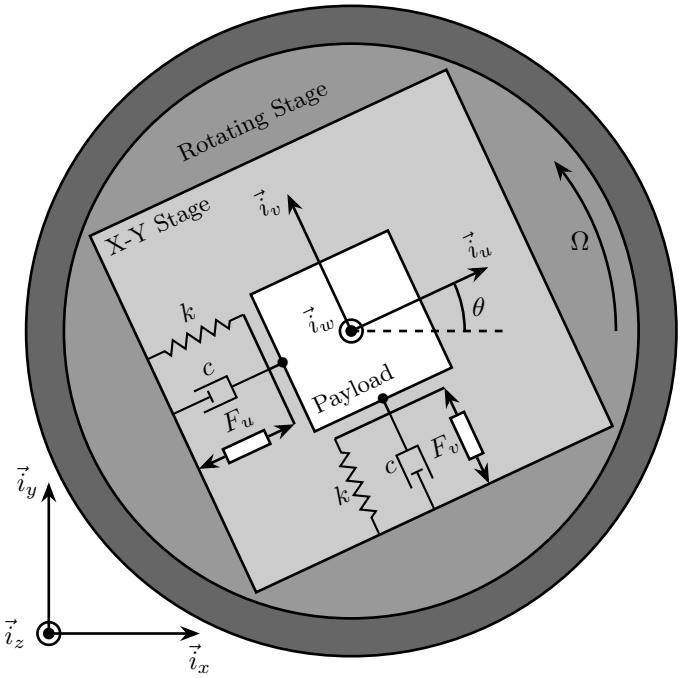

Figure 1: Schematic of the studied System

2.2 Equations of Motion

To obtain of equation of motion for the system represented in Figure 1, the Lagrangian equations are used:

$$\frac{d}{dt}\left(\frac{\partial L}{\partial \dot{q}_i}\right) + \frac{\partial D}{\partial \dot{q}_i} - \frac{\partial L}{\partial q_i} = Q_i \tag{1}$$

with $L = T - V$ the Lagrangian, D the dissipation function, and Q_i the generalized force associated with the generalized variable $\begin{bmatrix} q_1 & q_2 \end{bmatrix} = \begin{bmatrix} d_u & d_v \end{bmatrix}$.

The constant rotation in the $(\vec{i}_x, \vec{i}_y)$ plane is here disregarded as it is imposed by the rotating stage.

$$T = \frac{1}{2} m \left(\left(\dot{d}_u - \Omega d_v \right)^2 + \left(\dot{d}_v + \Omega d_u \right)^2 \right) \tag{2a}$$

$$V = \frac{1}{2} k \left({d_u}^2 + {d_v}^2 \right) \tag{2b}$$

$$D = \frac{1}{2} c \left({\dot{d}_u}^2 + {\dot{d}_v}^2 \right) \tag{2c}$$

$$Q_1 = F_u, \quad Q_2 = F_v \tag{2d}$$

Substituting equations (2) into (1) gives the two coupled differential equations:

$$m\ddot{d}_u + c\dot{d}_u + (k - m\Omega^2) d_u = F_u + 2m\Omega\dot{d}_v \tag{3a}$$

$$m\ddot{d}_v + c\dot{d}_v + (k \underbrace{- m\Omega^2}_{\text{Centrif.}}) d_v = F_v \underbrace{- 2m\Omega\dot{d}_u}_{\text{Coriolis}} \tag{3b}$$

The constant rotation of the system induces two Gyroscopic effects:

- Centrifugal forces: that can been seen as added negative stiffness along $\vec{i}_u$ and $\vec{i}_v$
- Coriolis Forces: that couples the motion in the two orthogonal directions

One can verify that without rotation ($\Omega = 0$) the system becomes equivalent as to two uncoupled one degree of freedom mass-spring-damper systems:

$$m\ddot{d}_u + c\dot{d}_u + kd_u = F_u \tag{4a}$$
$$m\ddot{d}_v + c\dot{d}_v + kd_v = F_v \tag{4b}$$

2.3 Transfer Functions in the Laplace domain

To study the dynamics of the system, the differential equations of motions (3) are transformed in the Laplace domain and the transfer function matrix from $\begin{bmatrix} F_u & F_v \end{bmatrix}$ to $\begin{bmatrix} d_u & d_v \end{bmatrix}$ is obtained:

$$\begin{bmatrix} d_u \\ d_v \end{bmatrix} = \boldsymbol{G}_d \begin{bmatrix} F_u \\ F_v \end{bmatrix} \tag{5}$$

with $\boldsymbol{G}_d$ a 2×2 transfer function matrix

$$\boldsymbol{G}_d = \begin{bmatrix} \frac{ms^2+cs+k-m\Omega^2}{(ms^2+cs+k-m\Omega^2)^2+(2m\Omega s)^2} & \frac{2m\Omega s}{(ms^2+cs+k-m\Omega^2)^2+(2m\Omega s)^2} \\ \frac{-2m\Omega s}{(ms^2+cs+k-m\Omega^2)^2+(2m\Omega s)^2} & \frac{ms^2+cs+k-m\Omega^2}{(ms^2+cs+k-m\Omega^2)^2+(2m\Omega s)^2} \end{bmatrix} \tag{6}$$

To simply the analysis, the following change of variable is performed:

- $\omega_0 = \sqrt{\frac{k}{m}}$: Undamped natural frequency of the mass-spring system in $\mathrm{rad/s}$
- $\xi = \frac{c}{2\sqrt{km}}$: Damping ratio

The transfer function matrix (6) becomes equal to

$$\boldsymbol{G}_d = \frac{1}{k} \begin{bmatrix} \frac{\frac{s^2}{{\omega_0}^2}+2\xi\frac{s}{\omega_0}+1-\frac{\Omega^2}{{\omega_0}^2}}{\left(\frac{s^2}{{\omega_0}^2}+2\xi\frac{s}{\omega_0}+1-\frac{\Omega^2}{{\omega_0}^2}\right)^2+\left(2\frac{\Omega}{\omega_0}\frac{s}{\omega_0}\right)^2} & \frac{2\frac{\Omega}{\omega_0}\frac{s}{\omega_0}}{\left(\frac{s^2}{{\omega_0}^2}+2\xi\frac{s}{\omega_0}+1-\frac{\Omega^2}{{\omega_0}^2}\right)^2+\left(2\frac{\Omega}{\omega_0}\frac{s}{\omega_0}\right)^2} \\ \frac{-2\frac{\Omega}{\omega_0}\frac{s}{\omega_0}}{\left(\frac{s^2}{{\omega_0}^2}+2\xi\frac{s}{\omega_0}+1-\frac{\Omega^2}{{\omega_0}^2}\right)^2+\left(2\frac{\Omega}{\omega_0}\frac{s}{\omega_0}\right)^2} & \frac{\frac{s^2}{{\omega_0}^2}+2\xi\frac{s}{\omega_0}+1-\frac{\Omega^2}{{\omega_0}^2}}{\left(\frac{s^2}{{\omega_0}^2}+2\xi\frac{s}{\omega_0}+1-\frac{\Omega^2}{{\omega_0}^2}\right)^2+\left(2\frac{\Omega}{\omega_0}\frac{s}{\omega_0}\right)^2} \end{bmatrix} \tag{7}$$

For all the numerical analysis in this study, $\omega_0 = 1\,\mathrm{rad\,s^{-1}}$, $k = 1\,\mathrm{N\,m^{-1}}$ and $\xi = 0.025 = 2.5\,\%$.

Even tough no system with such parameters will be encountered in practice, conclusions will be drawn relative to these parameters such that they can be generalized to any other parameter.

2.4 System Dynamics and Campbell Diagram

The poles of $\boldsymbol{G}_d$ are the complex solutions p of

$$\left(\frac{p^2}{{\omega_0}^2} + 2\xi\frac{p}{\omega_0} + 1 - \frac{\Omega^2}{{\omega_0}^2}\right)^2 + \left(2\frac{\Omega}{\omega_0}\frac{p}{\omega_0}\right)^2 = 0 \tag{8}$$

Supposing small damping ($\xi \ll 1$), two pairs of complex conjugate poles are obtained:

$$p_+ = -\xi\omega_0 \left(1 + \frac{\Omega}{\omega_0}\right) \pm j\omega_0 \left(1 + \frac{\Omega}{\omega_0}\right) \tag{9a}$$

$$p_- = -\xi\omega_0 \left(1 - \frac{\Omega}{\omega_0}\right) \pm j\omega_0 \left(1 - \frac{\Omega}{\omega_0}\right) \tag{9b}$$

The real part and complex part of these two pairs of complex conjugate poles are represented in Figure 2 as a function of the rotational speed Ω. As the rotational speed increases, p_+ goes to higher frequencies and p_- to lower frequencies. The system becomes unstable for $\Omega > \omega_0$ as the real part of p_- is positive. Physically, the negative stiffness term $-m\Omega^2$ induced by centrifugal forces exceeds the spring stiffness k.

In the rest of this study, rotational speeds smaller than the undamped natural frequency of the system are used ($\Omega < \omega_0$).

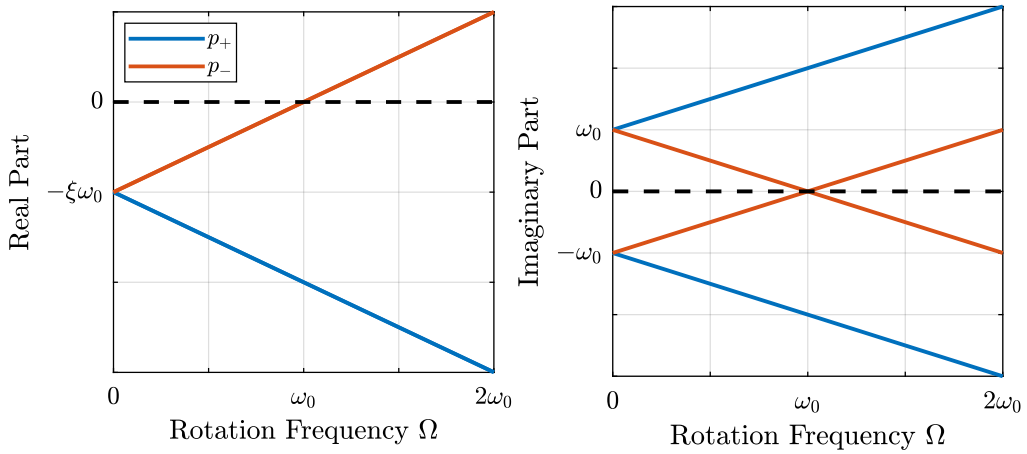

(a) Real Part (b) Imaginary Part

Figure 2: Campbell Diagram : Evolution of the complex and real parts of the system's poles as a function of the rotational speed Ω

Looking at the transfer function matrix $\boldsymbol{G}_d$ in Eq. (7), one can see that the two diagonal (direct) terms are equal and the two off-diagonal (coupling) terms are opposite. The bode plot of these two distinct terms are shown in Figure 3 for several rotational speeds Ω.

It is confirmed that the two pairs of complex conjugate poles are further separated as Ω increases. For $\Omega > \omega_0$, the low frequency complex conjugate poles p_- becomes unstable.

3 Decentralized Integral Force Feedback

3.1 Force Sensors and Control Architecture

In order to apply Decentralized Integral Force Feedback to the system, force sensors are added in series with the two actuators (Figure 4). Two identical controllers K_F are added to feedback each of the sensed forces to its collocated actuator. The control diagram is shown in Figure 5.

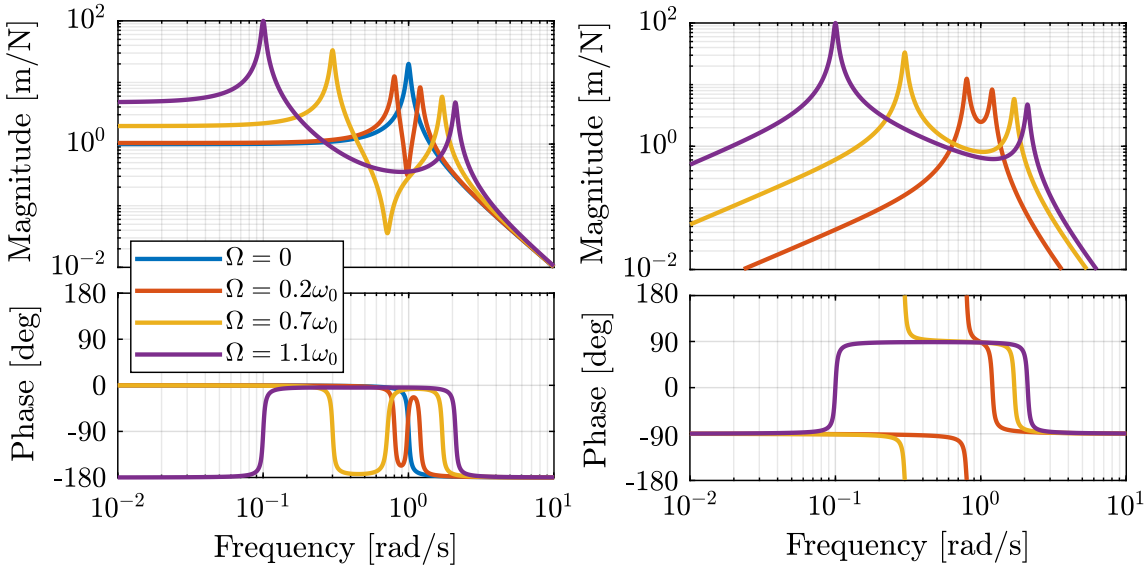

(a) Direct Terms d_u/F_u, d_v/F_v

(b) Coupling Terms d_v/F_u, $-d_u/F_v$

Figure 3: Bode Plots for $\boldsymbol{G}_d$ for several rotational speed Ω

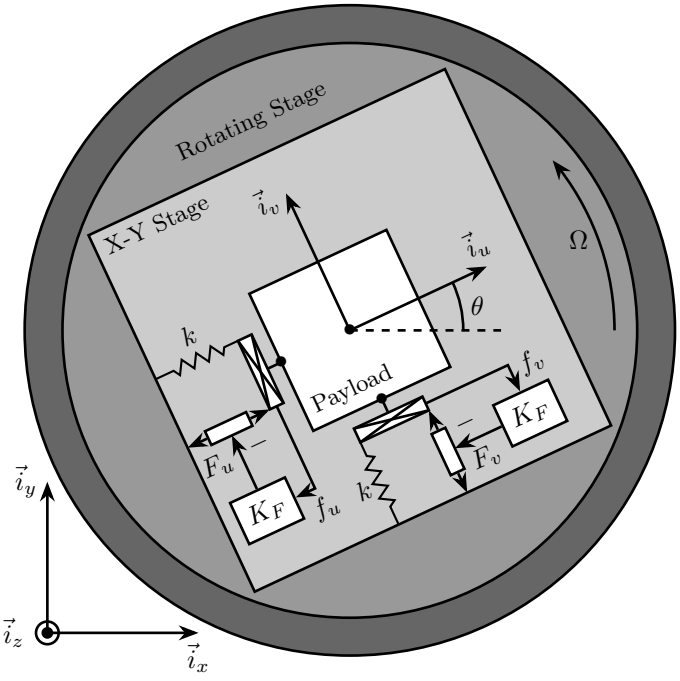

Figure 4: System with added Force Sensor in series with the actuators

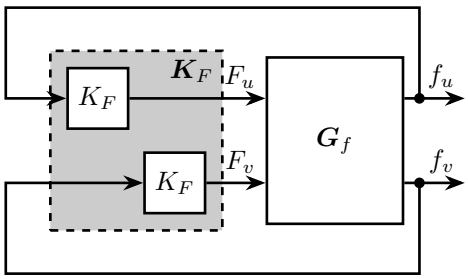

Figure 5: Control Diagram for decentralized IFF

3.2 Plant Dynamics

The forces measured by the force sensors are equal to:

$$\begin{bmatrix} f_u \\ f_v \end{bmatrix} = \begin{bmatrix} F_u \\ F_v \end{bmatrix} - (cs + k) \begin{bmatrix} d_u \\ d_v \end{bmatrix} \tag{10}$$

Re-injecting (7) into (10) yields:

$$\begin{bmatrix} f_u \\ f_v \end{bmatrix} = \boldsymbol{G}_f \begin{bmatrix} F_u \\ F_v \end{bmatrix} \tag{11}$$

with $\boldsymbol{G}_f$ a 2×2 transfer function matrix

$$\boldsymbol{G}_f = \begin{bmatrix} \frac{\left(\frac{s^2}{{\omega_0}^2} - \frac{\Omega^2}{{\omega_0}^2}\right)\left(\frac{s^2}{{\omega_0}^2} + 2\xi\frac{s}{\omega_0} + 1 - \frac{\Omega^2}{{\omega_0}^2}\right) + \left(2\frac{\Omega}{\omega_0}\frac{s}{\omega_0}\right)^2}{\left(\frac{s^2}{{\omega_0}^2} + 2\xi\frac{s}{\omega_0} + 1 - \frac{\Omega^2}{{\omega_0}^2}\right)^2 + \left(2\frac{\Omega}{\omega_0}\frac{s}{\omega_0}\right)^2} & \frac{-\left(2\xi\frac{s}{\omega_0} + 1\right)\left(2\frac{\Omega}{\omega_0}\frac{s}{\omega_0}\right)}{\left(\frac{s^2}{{\omega_0}^2} + 2\xi\frac{s}{\omega_0} + 1 - \frac{\Omega^2}{{\omega_0}^2}\right)^2 + \left(2\frac{\Omega}{\omega_0}\frac{s}{\omega_0}\right)^2} \\ \frac{\left(2\xi\frac{s}{\omega_0} + 1\right)\left(2\frac{\Omega}{\omega_0}\frac{s}{\omega_0}\right)}{\left(\frac{s^2}{{\omega_0}^2} + 2\xi\frac{s}{\omega_0} + 1 - \frac{\Omega^2}{{\omega_0}^2}\right)^2 + \left(2\frac{\Omega}{\omega_0}\frac{s}{\omega_0}\right)^2} & \frac{\left(\frac{s^2}{{\omega_0}^2} - \frac{\Omega^2}{{\omega_0}^2}\right)\left(\frac{s^2}{{\omega_0}^2} + 2\xi\frac{s}{\omega_0} + 1 - \frac{\Omega^2}{{\omega_0}^2}\right) + \left(2\frac{\Omega}{\omega_0}\frac{s}{\omega_0}\right)^2}{\left(\frac{s^2}{{\omega_0}^2} + 2\xi\frac{s}{\omega_0} + 1 - \frac{\Omega^2}{{\omega_0}^2}\right)^2 + \left(2\frac{\Omega}{\omega_0}\frac{s}{\omega_0}\right)^2} \end{bmatrix} \tag{12}$$

The zeros of the diagonal terms are equal to (neglecting the damping for simplicity)

$$z_c = \pm j\omega_0 \sqrt{\frac{1}{2}\sqrt{8\frac{\Omega^2}{{\omega_0}^2} + 1} + \frac{\Omega^2}{{\omega_0}^2} + \frac{1}{2}} \tag{13a}$$

$$z_r = \pm\omega_0 \sqrt{\frac{1}{2}\sqrt{8\frac{\Omega^2}{{\omega_0}^2} + 1} - \frac{\Omega^2}{{\omega_0}^2} - \frac{1}{2}} \tag{13b}$$

The frequency of the two complex conjugate zeros z_c (13a) is between the frequency of the two pairs of complex conjugate poles p_- and p_+ (9). This is the expected behavior of a collocated pair of actuator and sensor.

However for non-null rotational speeds, two real zeros z_r (13b) appear in the diagonal terms which represent a non-minimum phase behavior. This can be seen in the Bode plot of the diagonal terms (Figure 6) where the magnitude experiences an increase of its slope without any change of phase.

The low frequency gain of $\boldsymbol{G}_f$ is no longer zero, and increases with the rotational speed Ω

$$\lim_{\omega \to 0} |\boldsymbol{G}_f(j\omega)| = \begin{bmatrix} \frac{-\Omega^2}{{\omega_0}^2 - \Omega^2} & 0 \\ 0 & \frac{-\Omega^2}{{\omega_0}^2 - \Omega^2} \end{bmatrix} \tag{14}$$

This low frequency gain can be explained as follows: a constant force induces a small displacement of the mass, which then increases the centrifugal forces measured by the force sensors.

3.3 Decentralized Integral Force Feedback with Pure Integrators

The two IFF controllers K_F are pure integrators

$$\boldsymbol{K}_F(s) = \begin{bmatrix} K_F(s) & 0 \\ 0 & K_F(s) \end{bmatrix}, \quad K_F(s) = g \cdot \frac{1}{s} \tag{15}$$

where g is a scalar value representing the gain of the controller.

In order to see how the controller affects the poles of the closed loop system, the Root Locus is constructed as follows. The poles of the closed-loop system are drawn in the complex plane as the gain g varies from 0 to ∞ for the two controllers simultaneously. The closed-loop poles start at the open-loop poles (shown by ✖) for $g = 0$ and coincide with the transmission zeros (shown by ⭘) as $g \to \infty$. The direction of increasing gains is shown by the arrows ➤.

Whereas collocated IFF is known for its guaranteed stability, which is the case here for $\Omega = 0$, this property is lost as soon as the rotational speed in non-null due to gyroscopic effects. This can be seen in the Root Locus (Figure 7) where the pole corresponding to the controller is bounded to the right half plane implying closed-loop system instability.

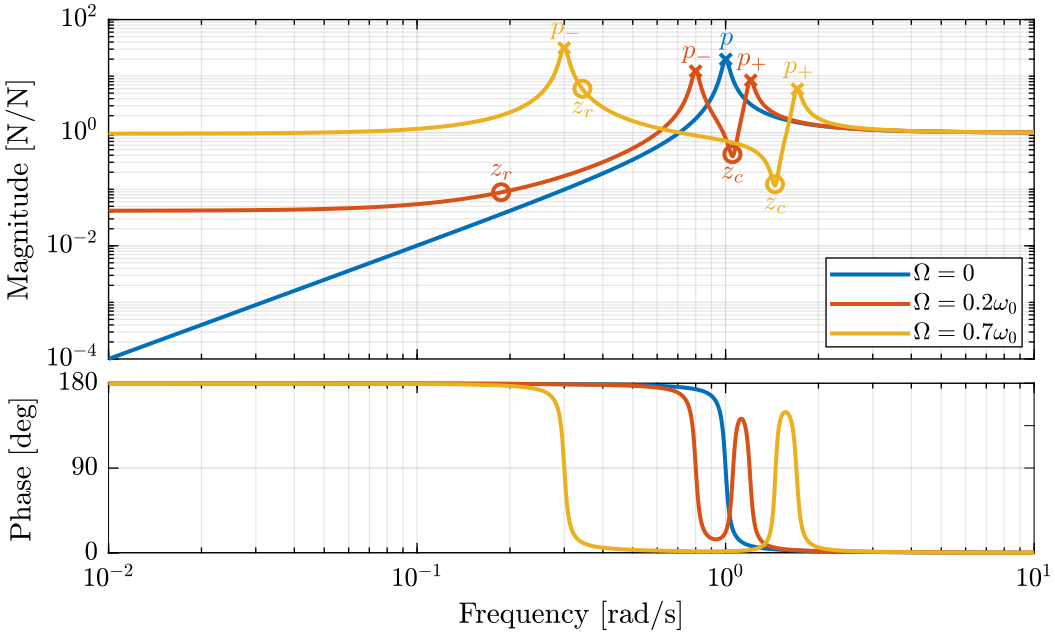

Figure 6: Bode plot of the diagonal terms of $\boldsymbol{G}_f$ for several rotational speeds Ω

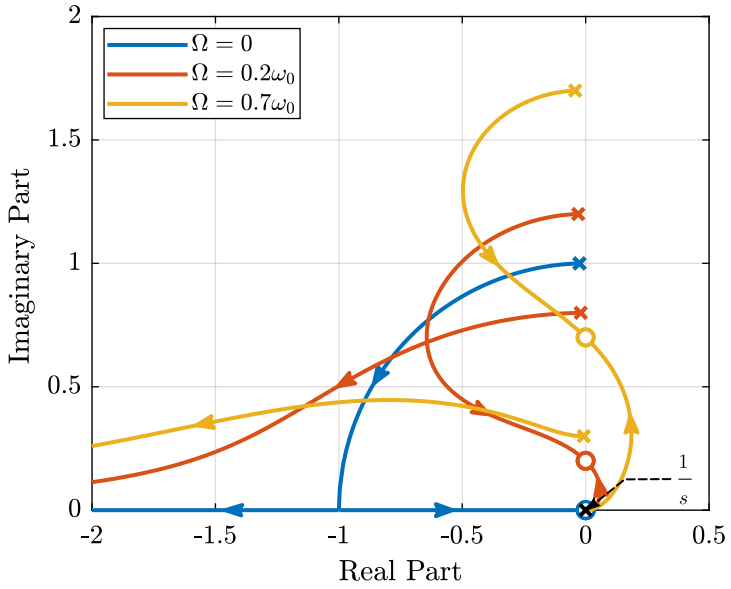

Figure 7: Root Locus for the Decentralized Integral Force Feedback

Two system modifications are proposed in the next sections to deal with this stability problem. Either the control law can be change (Section 4) or the mechanical system slightly modified (Section 5).

4 Integral Force Feedback with High Pass Filters

4.1 Modification of the Control Low

In order to limit the low frequency controller gain, an high pass filter (HPF) can be added to the controller which becomes

$$\boldsymbol{K}_F(s) = \begin{bmatrix} K_F(s) & 0 \\ 0 & K_F(s) \end{bmatrix}, \quad K_F(s) = g \cdot \frac{1}{s} \cdot \underbrace{\frac{s/\omega_i}{1 + s/\omega_i}}_{\text{HPF}} = g \cdot \frac{1}{s + \omega_i} \tag{16}$$

This is equivalent as to slightly shifting to controller pole to the left along the real axis. This modification of the IFF controller is typically done to avoid saturation associated with the pure integrator [2]. This is however not the case in this study as it will become in the next section.

4.2 Feedback Analysis

The loop gains for an individual decentralized controller $K_F(s)$ with and without the added HPF are shown in Figure 8. The effect of the added HPF is a limitation of the low frequency gain.

The Root Loci for the decentralized IFF with and without the HPF are displayed in Figure 9. With the added HPF, the poles of the closed loop system are shown to be stable up to some value of the gain g_{max}

$$g_{\text{max}} = \omega_i \left(\frac{{\omega_0}^2}{\Omega^2} - 1 \right) \tag{17}$$

This gain also corresponds as to when the low frequency loop gain reaches one.

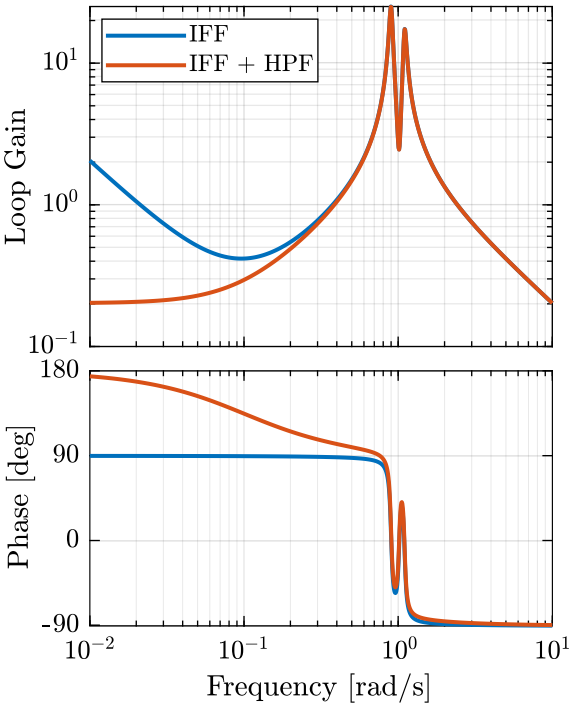

Figure 8: Modification of the loop gain with the added HFP, $g = 2$, $\omega_i = 0.1\omega_0$ and $\Omega = 0.1\omega_0$

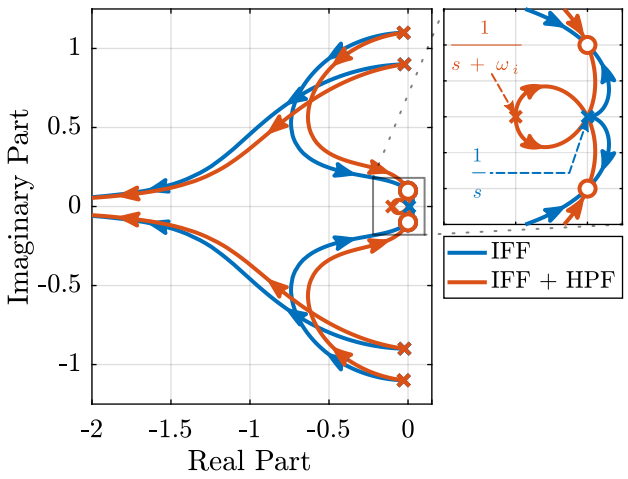

Figure 9: Modification of the Root Locus with the added HPF, $\omega_i = 0.1\omega_0$ and $\Omega = 0.1\omega_0$

4.3 Optimal Control Parameters

Two parameters can be tuned for the controller (16): the gain g and the location of the pole ω_i. The optimal values of ω_i and g are considered as the values for which the damping of all the closed-loop poles are simultaneously maximized.

The Root Loci for several ω_i are shown in Figure 10. It is shown that even tough small ω_i seems to allow more damping to be added to the system resonances, the control gain g may be limited to small values due to Eq. (17).

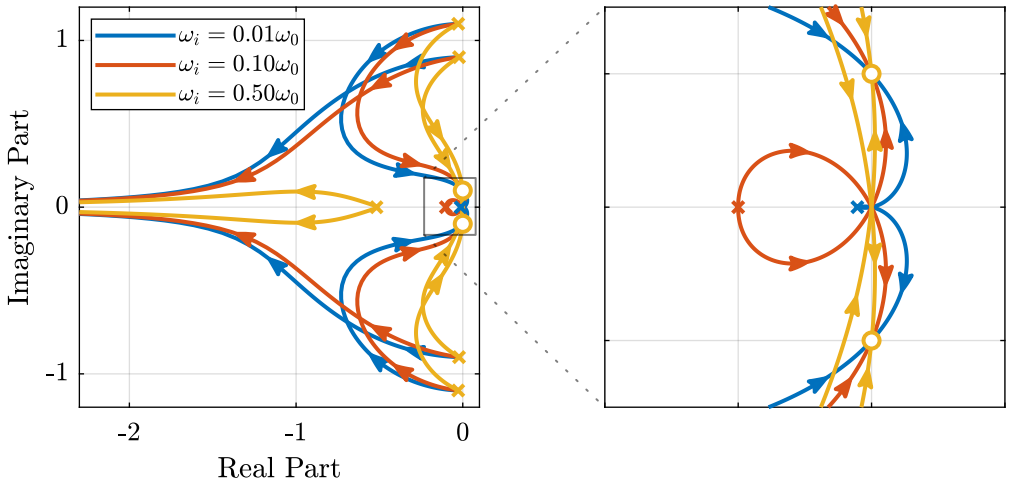

Figure 10: Root Locus for several HPF cut-off frequencies ω_i, $\Omega = 0.1\omega_0$

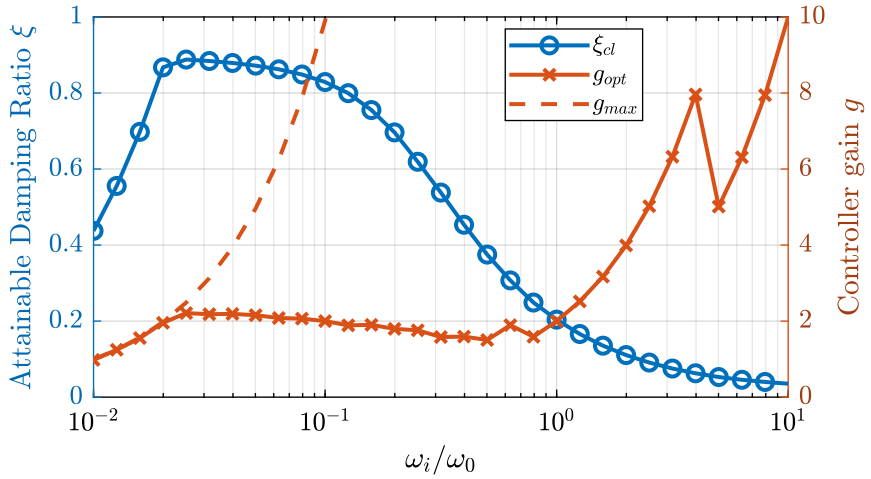

Figure 11: Attainable damping ratio ξ_{cl} as a function of the ratio ω_i/ω_0. Corresponding control gain g_{opt} and g_{max} are also shown

5 Integral Force Feedback with Parallel Springs

5.1 Stiffness in Parallel with the Force Sensor

As was shown in the previous sections, the instability when using Decentralized IFF for rotating positioning platforms is due to Gyroscopic effects, more precisely to the negative stiffnesses induced by centrifugal forces. The idea in this section is to include additional springs in parallel with the force sensors to counteract the negative stiffness due to centrifugal forces. Such springs are schematically shown in Figure 12 where k_a is the stiffness of the actuator and k_p the stiffness in parallel with the actuator and force sensor.

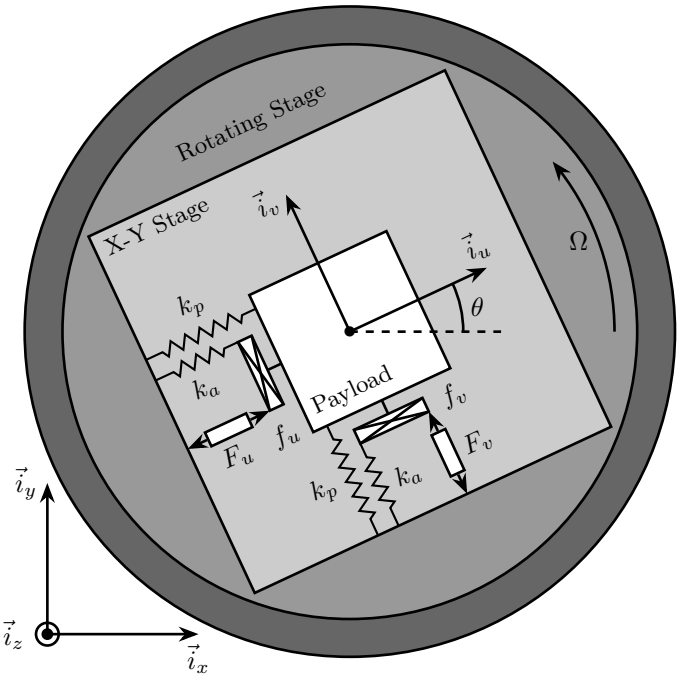

Figure 12: Studied system with additional springs in parallel with the actuators and force sensors

Figure 13: XY Piezoelectric Stage (XY25XS from Cedrat-Technology)

The forces measured by the force sensors are equal to:

$$\begin{bmatrix} f_u \\ f_v \end{bmatrix} = \begin{bmatrix} F_u \\ F_v \end{bmatrix} - (cs + k_a) \begin{bmatrix} d_u \\ d_v \end{bmatrix} \tag{18}$$

This could represent a system where

5.2 Effect of the Parallel Stiffness on the Plant Dynamics

We define an adimensional parameter α, $0 \leq \alpha < 1$, that describes the proportion of the stiffness in parallel with the actuator and force sensor:

$$k_p = \alpha k \tag{19a}$$
$$k_a = (1 - \alpha) k \tag{19b}$$

The overall stiffness k stays constant:

$$k = k_a + k_p \tag{20}$$

$$\begin{bmatrix} f_u \\ f_v \end{bmatrix} = \boldsymbol{G}_k \begin{bmatrix} F_u \\ F_v \end{bmatrix} \tag{21}$$

$$\boldsymbol{G}_k = \begin{bmatrix} \frac{\left(\frac{s^2}{{\omega_0}^2} - \frac{\Omega^2}{{\omega_0}^2} + \alpha\right)\left(\frac{s^2}{{\omega_0}^2} + 2\xi\frac{s}{\omega_0} + 1 - \frac{\Omega^2}{{\omega_0}^2}\right) + \left(2\frac{\Omega}{\omega_0}\frac{s}{\omega_0}\right)^2}{\left(\frac{s^2}{{\omega_0}^2} + 2\xi\frac{s}{\omega_0} + 1 - \frac{\Omega^2}{{\omega_0}^2}\right)^2 + \left(2\frac{\Omega}{\omega_0}\frac{s}{\omega_0}\right)^2} & \frac{-\left(2\xi\frac{s}{\omega_0} + 1 - \alpha\right)\left(2\frac{\Omega}{\omega_0}\frac{s}{\omega_0}\right)}{\left(\frac{s^2}{{\omega_0}^2} + 2\xi\frac{s}{\omega_0} + 1 - \frac{\Omega^2}{{\omega_0}^2}\right)^2 + \left(2\frac{\Omega}{\omega_0}\frac{s}{\omega_0}\right)^2} \\ \frac{\left(2\xi\frac{s}{\omega_0} + 1 - \alpha\right)\left(2\frac{\Omega}{\omega_0}\frac{s}{\omega_0}\right)}{\left(\frac{s^2}{{\omega_0}^2} + 2\xi\frac{s}{\omega_0} + 1 - \frac{\Omega^2}{{\omega_0}^2}\right)^2 + \left(2\frac{\Omega}{\omega_0}\frac{s}{\omega_0}\right)^2} & \frac{\left(\frac{s^2}{{\omega_0}^2} - \frac{\Omega^2}{{\omega_0}^2} + \alpha\right)\left(\frac{s^2}{{\omega_0}^2} + 2\xi\frac{s}{\omega_0} + 1 - \frac{\Omega^2}{{\omega_0}^2}\right) + \left(2\frac{\Omega}{\omega_0}\frac{s}{\omega_0}\right)^2}{\left(\frac{s^2}{{\omega_0}^2} + 2\xi\frac{s}{\omega_0} + 1 - \frac{\Omega^2}{{\omega_0}^2}\right)^2 + \left(2\frac{\Omega}{\omega_0}\frac{s}{\omega_0}\right)^2} \end{bmatrix} \tag{22}$$

$$\alpha > \frac{\Omega^2}{{\omega_0}^2} \Leftrightarrow k_p > m\Omega^2 \tag{23}$$

If the added stiffness is higher than the maximum negative stiffness, then the poles of the IFF damped system will stay in the (stable) right half-plane.

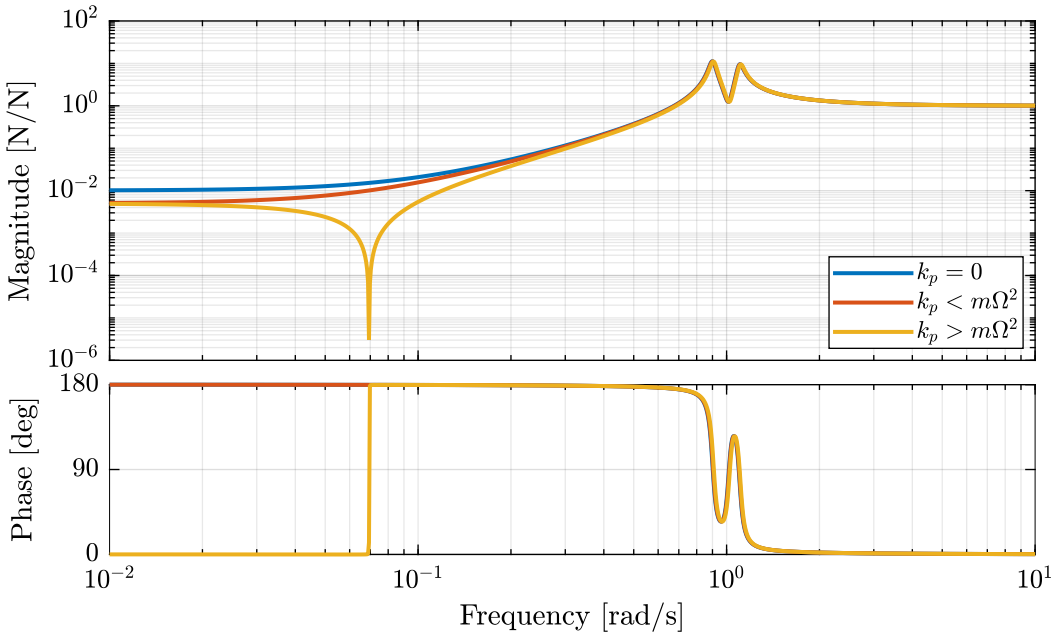

Figure 14: Bode Plot of f_u/F_u without parallel spring, with parallel springs with stiffness $k_p < m\Omega^2$ and $k_p > m\Omega^2$, $\Omega = 0.1\omega_0$

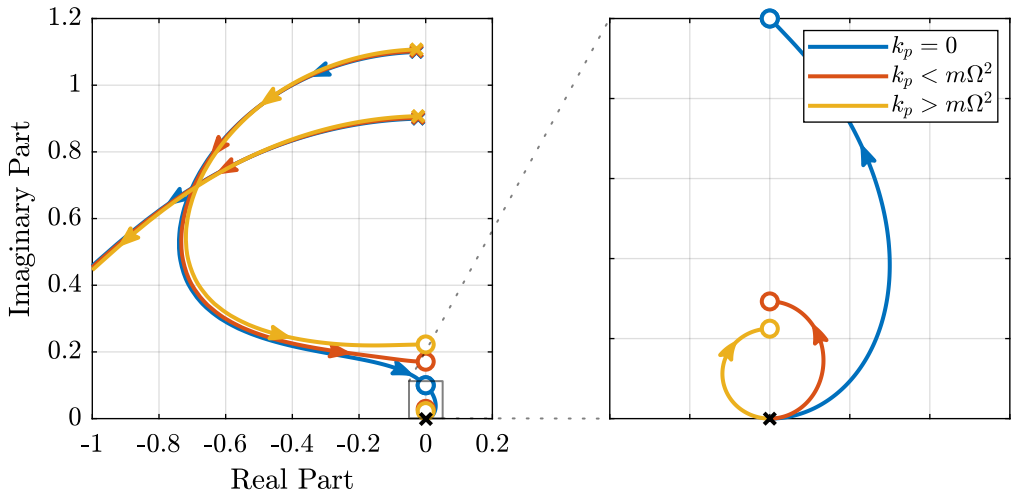

Figure 15: Root Locus for IFF without parallel spring, with parallel springs with stiffness $k_p < m\Omega^2$ and $k_p > m\Omega^2$, $\Omega = 0.1\omega_0$

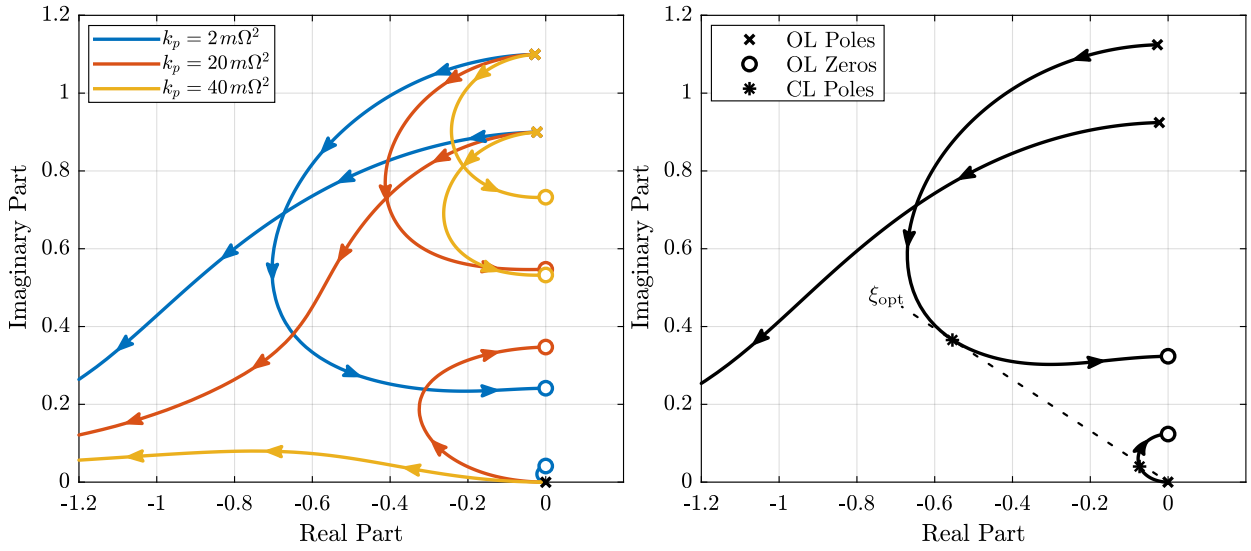

(a) Three values of k_p

(b) $k_p = 5m\Omega^2$, optimal damping is shown

Figure 16: Root Locus for IFF when parallel stiffness is used, $\Omega = 0.1\omega_0$

5.3 Optimal Parallel Stiffness

6 Comparison of the Proposed Active Damping Techniques for Rotating Positioning Stages

6.1 Physical Comparison

6.2 Attainable Damping

6.3 Transmissibility and Compliance

7 Conclusion

MIMO approach to study the coupling effects?

Acknowledgment

References

[1] T. Dehaeze, "Active damping of rotating positioning platforms," Source Code on Zonodo, 07 2020. [Online]. Available: https://doi.org/10.5281/zenodo.3894342

[2] A. Preumont, J.-P. Dufour, and C. Malekian, "Active damping by a local force feedback with piezoelectric actuators," in *32nd Structures, Structural Dynamics, and Materials Conference*. American Institute of Aeronautics and Astronautics, apr 1991. [Online]. Available: https://doi.org/10.2514/6.1991-989

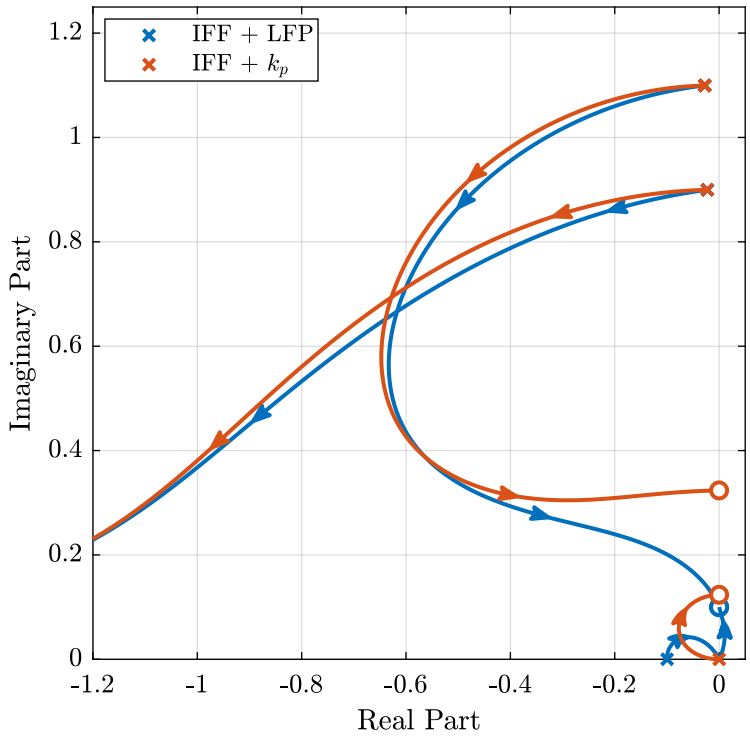

Figure 17: Root Locus for the three proposed decentralized active damping techniques: IFF with HFP, IFF with parallel springs, and relative DVF, $\Omega = 0.1\omega_0$

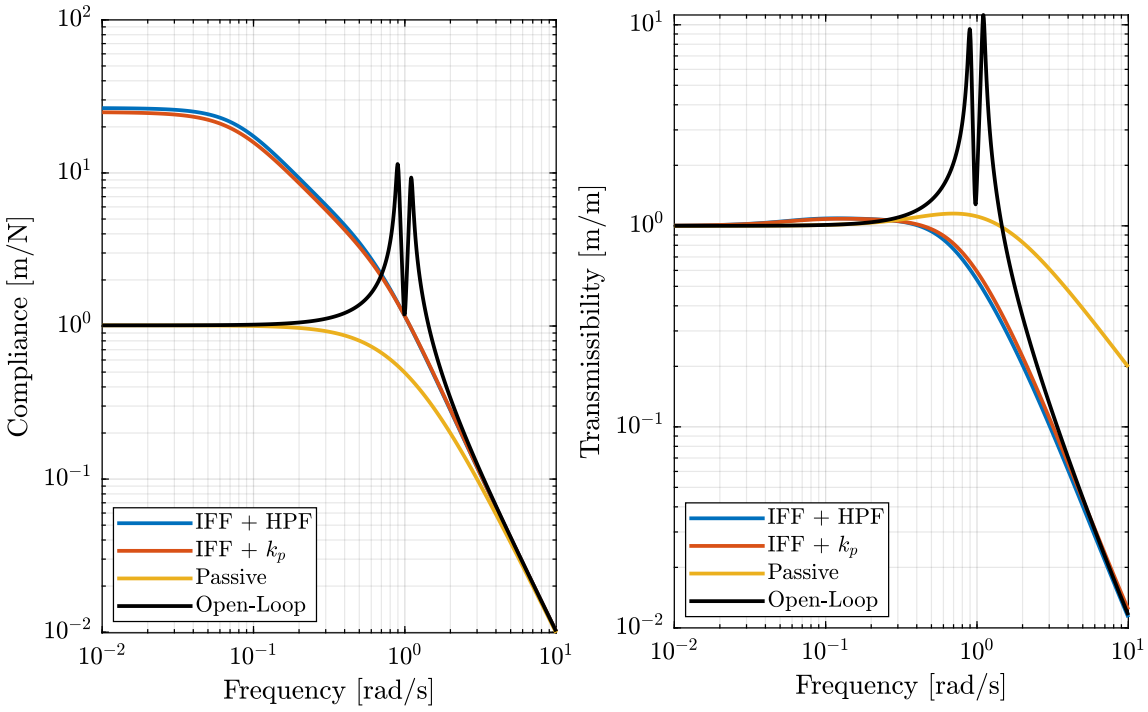

(a) Transmissibility

(b) Compliance

Figure 18: Comparison of the two proposed Active Damping Techniques, $\Omega = 0.1\omega_0$